Synthesis of Vanillin from Biomass-Derived Isoeugenol Using Immobilized Cobalt-Porphyrin on Hydroxyl-rich Graphene Oxide Catalyst

Kaiprathu Anjali [a*], Shun Nishimura[a,b*]

[a]*Graduate School of Advanced Science and Technology, Japan Advanced Institute of Science and Technology, 1-1 Asahidai, Nomi, Ishikawa 923-1292, Japan*

[b]*Research Center for Carbon Neutral, Japan Advanced Institute of Science and Technology, 1-1 Asahidai, Nomi, Ishikawa 923-1292, Japan*

**Email: anjaliballa123@gmail.com, anjali@jaist.ac.jp (KA); s_nishim@jaist.ac.jp (SN)*

ABSTRACT

Synthesis of vanillin from isoeugenol by oxidation has been investigated using cobalt(II) porphyrin (CoTCPP: meso-tetrakis(4-carboxy)phenyl porphyrinato cobalt(II)) covalently linked to hydroxyl-rich graphene oxide (GOOH) as a heterogeneous catalyst. The catalyst was thoroughly characterized by various spectroscopic techniques, such as FT-IR, XRD, N_2 adsorption-desorption, XPS, and SEM-EDS analytical techniques. Catalytic activity of the CoTCPP/GOOH gave an excellent yield of 75.1% in the conversion of isoeugenol to vanillin using molecular oxygen for 20 h reaction at 100 °C in 3.0 MPa oxygen pressure. The catalyst showed exceptional stability upon multiple reuses without significant loses in activity. Accordingly, the present study highlights the promise of CoTCPP/GOOH as a heterogeneous catalyst for the efficient aerobic oxidation of biomass-derived platform chemicals into valuable end-products.

KEYWORDS: porphyrin; graphene oxide; biomass; oxidative cleavage; isoeugenol; vanillin

INTRODUCTION

The depletion of non-renewable energy sources in nature, coupled with the excessive emission of greenhouse gases from petroleum materials, has intensified the energetic and environmental challenges.[1,2] As energy demands continue to rise, there is an urgent need to address these issues. Biomass emerges as a compelling solution due to its robust regenerative qualities, cleanliness, and abundant presence in nature.[3] In both the field of green chemistry and broader academic and industrial research domains, the conversion of lignocellulosic biomass into value-added chemicals has become a focal point.[4] Inedible biomass stands out as a sustainable and appealing

renewable feedstock, offering potential for the production of drop-in liquid fuels and bio-products with high carbon efficiency.[5] Recognizing the importance of transitioning towards sustainable energy practices, researchers are increasingly focusing on developing innovative technologies to produce fuels and chemicals from renewable energy resources. Among these resources, biomass, with its carbonaceous energy potential, holds particular promise for the production of transportation fuels and platform chemicals.[6] This collective effort signifies a pivotal step towards addressing the dual challenges of energy security and environmental sustainability. Within this context, catalytic oxidation of biomass-derived intermediates has garnered significant attention. In particular, lignocellulose-derived compounds such as glucose, furfural, 5-hydroxymethylfurfural (HMF), eugenol, and isoeugenol are being targeted for conversion into high-value chemicals.[7–9]

Among these compounds, isoeugenol stands out as a promising renewable feedstock for the synthesis of vanillin[10], a metabolite widely employed in food, cosmetics, pharmaceuticals, and performance products for its flavor, fragrance, and monomeric properties.[11–13] Natural vanillin, extracted through a labor-intensive process from vanilla beans, poses significant economic challenges due to the expensive cultivation of vanilla orchids and bean harvesting.[14,15] Consequently, researchers have turned their attention to derived lignin compounds such as eugenol, isoeugenol, and ferulic acid to streamline the production of vanillin through a straightforward oxidation pathway.[16,17] Vanillin, chemically known as 4-hydroxy-3-methoxybenzaldehyde, holds immense value across various industries due to its pivotal role as a flavor and aroma enhancer in vanilla-based products.[18,19] However, the majority of vanillin production currently relies on petrochemical-derived compounds, such as guaiacol and glyoxylic acid, through environmentally-unfriendly synthetic routes, resulting in low quality final products.[20–22] In addition, the natural extracts contribute only a small fraction, around 40-60 tons, to the total global supply of vanillin, which stands at 18,000 tons per year. This shortfall is due to high demand and supply imbalances from natural sources, leading to the majority of vanillin being produced synthetically.[23,24] Hence, there's growing interest in using isoeugenol derived from biomass lignin as a renewable carbon source for vanillin production. Isoeugenol, sourced from various plants including clove oil, presents a promising avenue. Despite its potential, the biotransformation of isoeugenol to vanillin has shown limited yields, primarily due to the complexity of the process, hindering industrial-scale production.[17,25,26] Recent research has explored alternative routes, such as photo-catalytic oxidation of trans-ferulic acid[27] and a three-step process using *p*-cresol, to produce vanillin.[28] However, some methods involve environmentally hazardous reagents like bromine. To address this, researchers have developed

safer catalytic processes using materials like TiO_2 and Bi_2WO_6 for oxidation[29], as well as Bu_4NVO_3/pyrazine-2-carboxylic acid[30] and Co-salen based catalysts[31]. Despite progress, the use of homogeneous catalysts and hazardous reagents, particularly bromine, remains a concern due to its adverse environmental impact.

Among various homogeneous catalysts, metalloporphyrins, renowned for their catalytic prowess analogous to cytochrome P-450 enzymes, exhibit promising potential in catalysing various oxidation reactions.[32,33] Among them, Co–porphyrins display remarkable oxygen-binding activity, making them efficient catalysts for oxidation.[34,35] However, their susceptibility to solution instability poses a significant challenge. To address this limitation, strategies involving the intercalation of metalloporphyrins into layered inorganic supports like clay minerals have been explored, offering avenues for enhancing stability and preventing catalyst deactivation.[36–38] Leveraging the unique properties of metalloporphyrins, particularly Co–porphyrins, holds immense promise in advancing catalytic processes for isoeugenol oxidation.

In the pursuit of sustainable vanillin production methods, graphene oxide (GO) emerges as a versatile platform for catalytic applications. Chemical reduction of GO yields reduced graphene oxide (rGO), preserving essential oxygen functionalities crucial for catalytic activity.[39,40] Harnessing the catalytic potential of rGO, recent studies have investigated its integration with Cu nanoparticles, demonstrating promise in lignin oxidation to vanillin.[41] Building upon this foundation, our study explores the synergistic potential of Co-porphyrin immobilized on hydroxyl-rich graphene oxide for the oxidation of isoeugenol to vanillin. By capitalizing on the unique properties of both Co-porphyrin and graphene oxide, we aim to develop a robust and efficient catalytic system, paving the way for sustainable vanillin synthesis while upholding environmental compatibility. In response, greener strategies leveraging the catalytic oxidation of isoeugenol have been developed and employing as an efficient catalyst to overcome these drawbacks and enable a more sustainable approach to vanillin production. Herein, we report the immobilization of isolated tetrakis(4-carboxy)phenyl porphyrinato cobalt(II) (CoTCPP) into a hydroxyl-rich graphene oxide support (GOOH). Considering that Co is commonly employed as active sites for oxidation reactions. The synthesized CoTCPP/GOOH was explored for its superior catalytic performance in the oxidative cleavage of biomass-derived isoeugenol to vanillin.

EXPERIMENTAL SECTION

Materials

All the chemicals and their details are listed in **Table S1**, in the Supporting Information. The cobalt-porphyrin (CoTCPP), hydroxyl rich graphene oxide (GOOH), and the immobilization of cobalt-porphyrin on hydroxyl-rich graphene oxide were prepared in the laboratory as described below.

Catalyst Preparation

Synthesis of meso-tetrakis(4-carboxy)phenyl porphyrinato cobalt(II) (CoTCPP)

The CoTCPP was synthesized by adapting a previously reported protocol.[42] In general, meso-tetrakis(4-carboxyphenyl)porphyrin (0.4 mmol), and $Co(OAc)_2 \cdot 4H_2O$ (2.4 mmol) were dissolved in 40 mL of *N*,*N*-dimethylformamide (DMF) subjected to refluxing for 2 h. Thereafter, the mixture was cooled to room temperature (25 °C) and precipitated with water (300 mL), and then the crude product was filtered, washed with water, and vacuum-dried at room temperature. The resulting material was recrystallized from a chloroform ($CHCl_3$) and hexane mixture (1:5, v/v) and vacuum-dried for 10 h. Finally, a yield of 0.182 g (84%) was obtained.

Synthesis of hydroxyl-rich graphene oxide (GOOH)

Graphene oxide (GO) is typically synthesized through the oxidation of graphite, resulting in the introduction of various oxygen-containing functional groups such as epoxides, hydroxyls, and carboxyls. However, the hydroxyl-rich graphene oxide (GOOH) contains a higher concentration of hydroxyl (-OH) groups on its surface, which can be achieved through the water-addition modified Hummers method as reported previously in the literature.[43] In the typical procedure, a 250 mL flask immersed in an ice bath, 46 mL of concentrated sulfuric acid was diluted by 12 mL of water with vigorous stirring (200 rpm). Once the solution is cooled below 10 °C, add 1.0 g of graphite powder. Slowly introduce 3.0 g of $KMnO_4$ into the suspension while ensuring that the temperature remains below 20 °C. Transfer the reaction system to a 40 °C oil bath and stir at 300 rpm for 2 h. Gradually pour the mixture into a 300 mL ice/water mixture while maintaining the temperature below 10 °C. Stir the resulting solution for 15 min, and then add 5 mL of 30% H_2O_2 drop by drop, observing the solution change from dark brown to yellow. Allow the suspension to stand undisturbed overnight. Filter the mixture and wash the resulting solid three times with 10% HCl solutions (50 mL each) to remove metal ions. Dry the resulting solid in a vacuum at room temperature to obtain the GOOH.[43]

Preparation of CoTCPP-immobilized GOOH

A total of 1.0 g of as-prepared GOOH was dispersed in 50 mL of *N*,*N*-dimethylformamide (DMF), followed by the addition of 0.7 g of CoTCPP, 400 mg of 2-(1H-benzotriazole-1-yl)-1,1,3,3-tetramethyluronium tetrafluoroborate (TBTU), and 300 mg of *N*,*N*-

diisopropylethylamine (DIPEA).[44,45] The resulting mixture was gently stirred for a duration of 48 h at room temperature. After completion of the reaction, the dark solid product was carefully separated by filtration and underwent multiple rinses with DMF. This washing step was crucial for removing any weakly-adsorbed metalloporphyrins from the hydroxyl-rich graphene oxide support, thereby ensuring the purity of the final product. Subsequently, the CoTCPP-immobilized GOOH material was allowed to air-dry in a vacuum at room temperature, resulting in the formation of a stable and functionalized composite material. This meticulous synthesis protocol yielded a high-quality CoTCPP-immobilized GOOH material suitable for various applications.

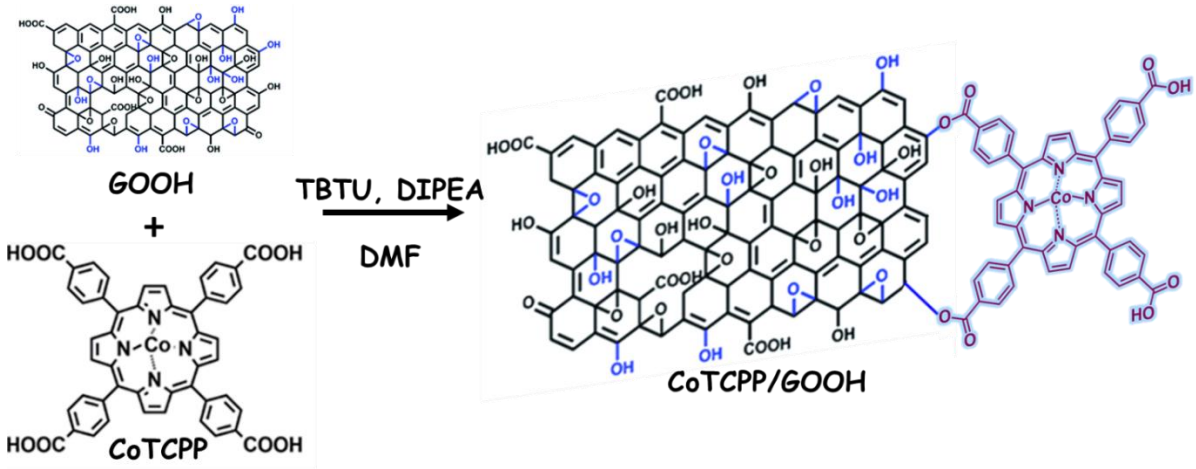

Scheme 1: Schematic representation of as-prepared CoTCPP/GOOH conformation.

General procedure for oxidation of isoeugenol

A stainless-steel autoclave reactor (EYELA RIKAKIKAI Co., Ltd., Japan, 20 mL vol.) with an internal Teflon vessel was charged with 1.0 mmol of isoeugenol, 20 mg of as-prepared CoTCPP/GOOH catalyst, and 3 mL of acetonitrile as the solvent. The autoclave was then repeatedly flushed with oxygen gas to keep the reactor's pressure at 3.0 MP at room temperature. The autoclave was heated for 20 h at 100 °C on an aluminum block bath (Zodiac CCX-CTRL2; EYELA RIKAKIKAI Co., Ltd., Japan) with constant stirring. The end product of the reaction was collected, centrifuged, filtered, and then subjected to analysis using a gas chromatography (Shimadzu GC-2014) with a non-polar DB-1 column (50 m, Agilent). The products were further confirmed by a GC-TOFMS (JEOL AccuTOF GCX) using an HP-5 column (30 m, Agilent). The conversion and selectivity were calculated using the following equations:

$$\boldsymbol{Conversion}\ (\%) = \frac{\boldsymbol{Moles\ of\ Isoeugenol\ consumed}}{\boldsymbol{Moles\ of\ initial\ Isoeugenol}}\ \boldsymbol{X\ 100}$$

$$\textbf{\textit{Yield of Product}}\ (\%) = \frac{\textbf{\textit{Moles of the Product}}}{\textbf{\textit{Moles of initial Isoeugenol}}}\ \textbf{\textit{X}}\ \mathbf{100}$$

Characterization methods

In this study, Fourier transform infrared spectroscopy (FT-IR) spectra were obtained using the PerkinElmer Spectrum 100 FT-IR Spectrometer. The measurements were performed in the range of 500–4000 cm^{-1} using the Attenuated Total Reflectance (ATR) method. The spectra were collected with a resolution of 4.0 cm^{-1} and 120 scans were acquired. Powder X-ray diffraction patterns were collected using a Rigaku MiniFlex X-Ray diffractometer through Cu Kα radiation with a wavelength of 1.54 Å, using a scanning speed of 4.0 degrees per minute and a step size of 0.01 degrees. The diffraction angles were measured in the range of 7–75 degrees. All sample was stabilized on the silicon non-reflective sample plate for the XRD measurement. N_2-adsorption-desorption studies were conducted using a BELSORP-mini analyser (MicrotracBEL, Corp.). The N_2 sorption measurements were performed at a temperature of 77 K by immersing the sample in a liquid N_2 bath. Before each run, the samples were degassed under a vacuum for 3 h at 110 °C. Scanning Electron Microscopy (SEM) and Energy-dispersive X-ray spectroscopy (EDS) mapping were conducted using a Hitachi TM3030 plus Desktop SEM operating at 15 kV. The sample size ranged from 2 to 5 mg, and the corresponding weight loss was recorded. The UV–visible (UV–vis) absorption spectra of the materials were acquired in the 800–200 nm region using the Jasco V770 spectrometer. X-ray photoelectron spectroscopy (XPS) was employed to examine the chemical composition and chemical state of individual elements. The measurements were performed using an Axis-Ultra DLD spectrometer system (Shimadzu Co. and Kratos Analytical Ltd.) with a monochromatic Al Kα X-ray source (1486.6 eV). The C 1s peak of the carbon nanotubes, which has a BE of 284.4 eV, was utilized to calibrate the binding energies. The peak deconvolutions were performed with the aid of XPSPEAK 4.1.

RESULTS AND DISCUSSION

Characterization of the catalyst

The FT-IR spectra of CoTCPP, hydroxyl-rich graphene oxide and CoTCPP immobilized on hydroxyl-rich graphene oxide are presented in **Figure 1**. The observed peaks at 1028, 1224, 3240 and 1723 cm^{-1} can be attributed to the C–O–C (epoxy), C–O, O-H, and C=O (carbonyl and carboxylic) functional groups inherently present in the hydroxyl-rich graphene oxide (GOOH).[42,46,47] Furthermore, the stretching band at 3240 cm^{-1} corresponds to O–H stretching,

a clear indicator of the OH-rich graphene oxide,[43] and it is not observed in the pristine graphene. While, a novel peak at 1600 cm^{-1} aligns with the C=C vibrational mode characteristic of the porphyrin moiety.[42,46,47] The presence of distinctive peaks at 1420 cm^{-1} and 1008 cm^{-1} is attributed to the bending vibrations of the C=N bond within the porphyrin ring and the Co–N stretching, respectively.[42] These findings collectively provide strong evidence for the successful grafting of cobalt-porphyrins onto the OH- rich graphene oxide support. Notably, at approximately 1723 cm^{-1}, we observed a broad C=O stretching band, while at 860 cm^{-1}, the C–H stretching of the pyrrole ring was evident.[46,47] The shift of the C=O stretch from 1723 cm^{-1} to 1698 cm^{-1} in the CoTCPP/GOOH composite convincingly confirms the formation of a covalent linkage between CoTCPP and GOOH. In addition, the presence of week C=O bond signals also suggests that carboxylic moieties of the CoTCPP participated in linking to the support material, GOOH via hydroxyl groups.[42]

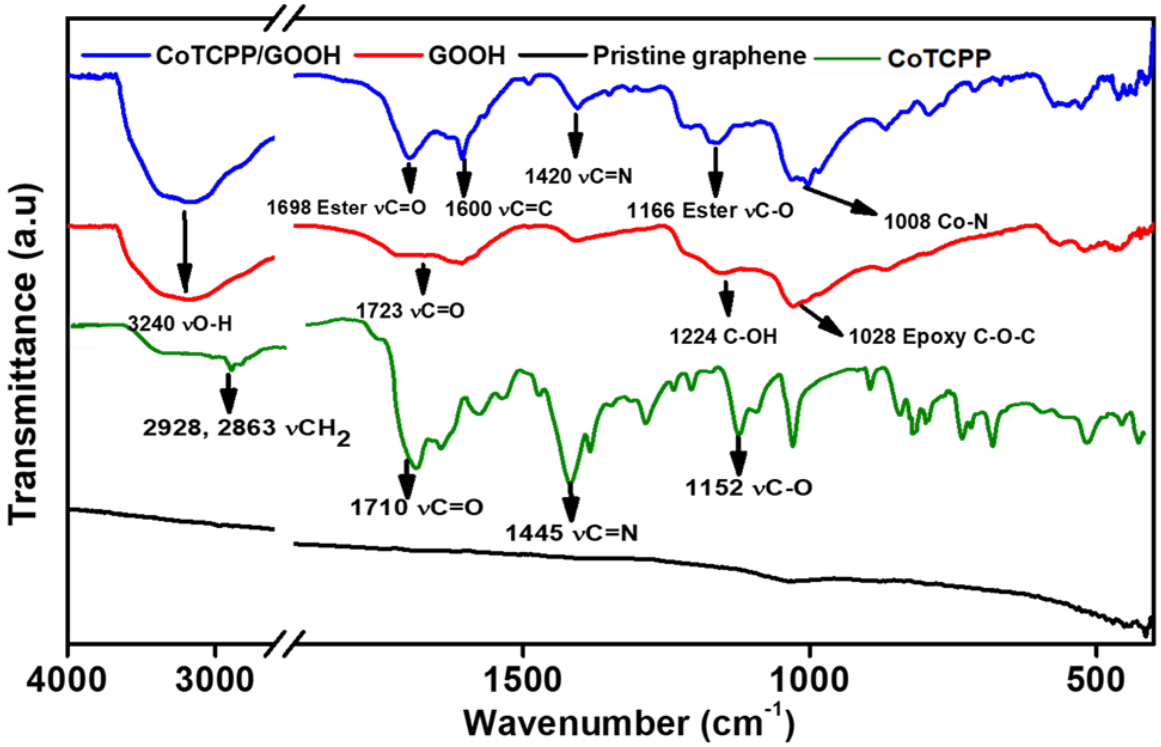

Figure 1. FT-IR spectra of pristine graphene, meso-tetrakis(4-carboxyphenyl)porphyrin (CoTCPP), hydroxyl-rich graphene oxide (GOOH), and CoTCPP immobilized on GOOH (CoTCPP/GOOH).

The powder X-ray diffraction (XRD) analysis was conducted to investigate the crystalline structures of the CoTCPP/GOOH preparation. In **Figure 2**, a pronounced peak at 2θ = 26.5º, corresponding to the (002) plane with an interlayer distance of 3.35 Å, is evident. The GOOH displays sharp diffraction peaks at 2θ = 10.06º, indicative of the (010) plane, with an interlayer

distance of approximately 8.78 Å. Notably, the (002) plane peak exhibits a shift compared to pristine graphene, occurring at 2θ = 27.08º, possibly due to the interaction of oxygenated functional groups in the OH-rich graphene oxide.[43] The CoTCPP/GOOH exhibits a peak at 2θ = 9.44º with an interlayer distance of 10.92 Å, suggesting an expansion of the (010) plane likely induced by the presence of porphyrin species. The expanded interlayer distance is notably smaller than the longest atom-to-atom distance within the cobalt-porphyrin molecules (e.g., the distance from one carboxylic group to its opposite is 15 Å).[48–50] This implies that covalent linkage between CoTCPP and GOOH through their carboxylate functional groups in cobalt-porphyrin and hydroxyl (OH) groups in OH- rich graphene oxide.

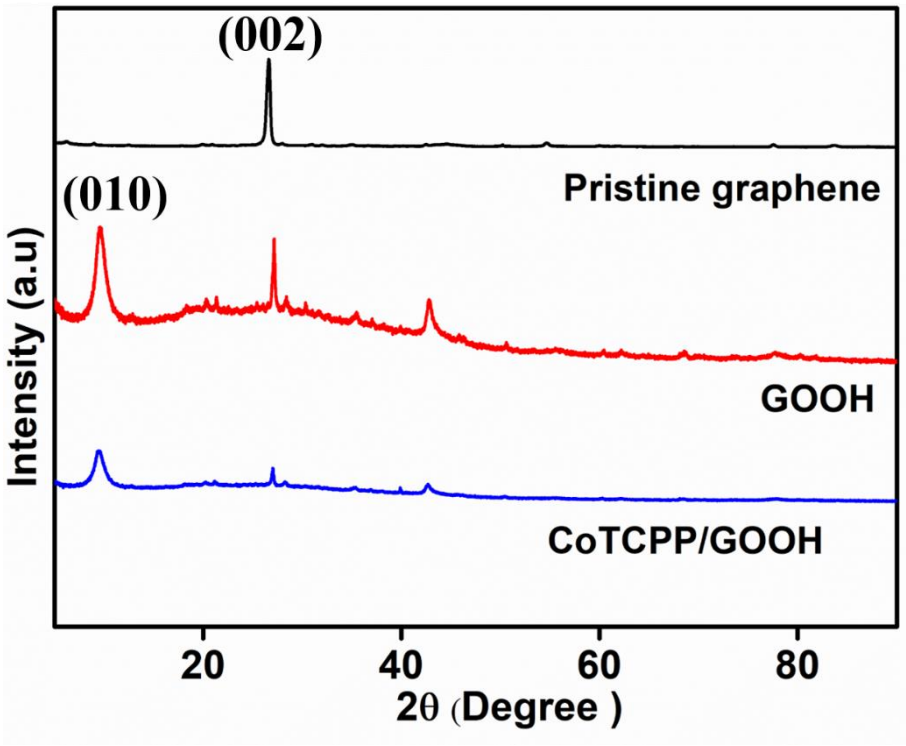

Figure 2. Powder XRD pattern of pristine graphene, hydroxyl-rich graphene oxide (GOOH), and CoTCPP immobilized on GOOH (CoTCPP/GOOH).

To elucidate the dispersion of cobalt-porphyrin on the hydroxyl-rich graphene oxide (GOOH) surface, element maps of the CoTCPP/GOOH are presented in **Figure 3**, which contains carbon (C) oxygen (O), nitrogen (N), and cobalt (Co). Notably, the SEM-EDX data shows that the C density in CoTCPP/GOOH; 66 wt%, is higher than that of C in GOOH; 43

wt%, as listed in **Table 1**. This is due to the functionalization between GOOH and CoTCPP, and which makes the C element become higher in CoTCPP/GOOH.

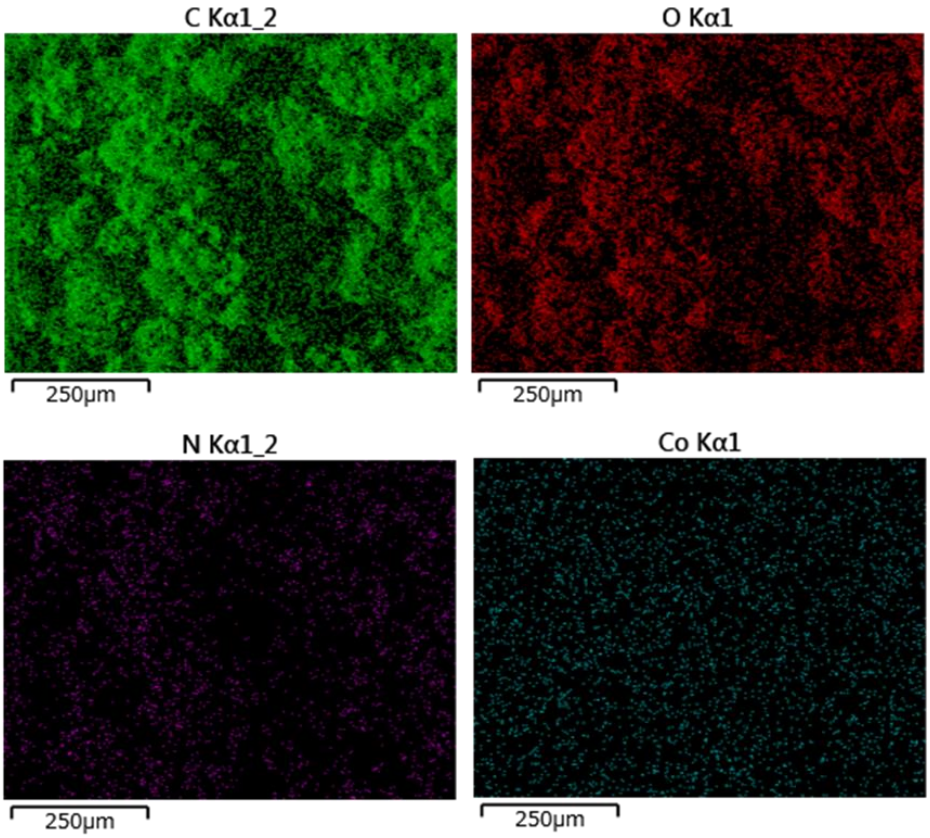

Figure 3. SEM-EDX elemental mapping for C, N, O, and Co elements in CoTCPP/GOOH.

The N_2 adsorption-desorption isotherms of GOOH and CoTCPP/GOOH exhibit a type IV isotherm corresponding to the mesoporous materials, as shown in **Figure S2**, in the Supporting Information. The specific surface area of the synthesized composites was determined through Brunauer–Emmett–Teller (BET) surface area analysis, and the results are presented in **Table 1**. The specific surface area of CoTCPP/GOOH is reported as 859 $m^2\ g^{-1}$, which is lower than that of hydroxyl-rich graphene oxide (GOOH) at 1207 $m^2\ g^{-1}$. This decrease in surface area implies effective immobilization of the cobalt-porphyrin on the OH-rich graphene oxide surface.

Further, the XPS spectrum provides valuable insights into the chemical functionalization in CoTCPP/GOOH. The wide scan XPS spectra of CoTCPP/GOOH is shown in **Figure 4a,** where distinct peaks corresponding to C 1s, N 1s, O 1s, and Co 2p are present. The high-resolution C 1s, N 1s, and Co 2p of CoTCPP/GOOH are shown in **Figure 4b, 4c, 4d and 4e**, respectively**.**

The C 1s can be deconvoluted into three peaks arising from sp^2 carbon at 284.6 eV, sp^3 carbon at 286.8 eV, and –C=O/–O–C=O at 288.1 eV[51], respectively **(Figure 4b).** Meanwhile, the high-resolution N 1s spectrum is deconvoluted into two peaks **(Figure 4c).** The peak obtained at 400.2 eV can be ascribed to the four chemically-equivalent metallic nitrogen atoms in the inner core of the Co-porphyrin (N-Co) bonding and the peak at 398.2 corresponds to the pyrolic N (N-C/N=C) origin. The O 1s spectrum **(Figure 4d)** is deconvoluted into four peaks, in which 529.3 eV, 530.4 eV, 532.1 eV and 533.2 eV respectively corresponds to –OH/–COOH, epoxy oxygen (–O–), –C=O/–COOH, and C–OH groups present in the CoTCPP/GOOH. The Co 2p high-resolution spectra **(Figure 4e)** show characteristic peaks at 780.1 eV and 796.3 eV corresponding to Co $2p_{3/2}$ and $2p_{1/2}$ along with satellite peaks. The separation of parent peaks by 16.2 eV indicates that the Co is in the Co^{+2} state.[52] These observations collectively confirm the successful grafting of cobalt-porphyrin onto the GOOH surface.

Table 1. Physicochemical properties of pristine graphene, hydroxyl-rich graphene oxide (GOOH) and cobalt-porphyrin immobilized on OH-rich graphene oxide (CoTCPP/GOOH).

Sample	Loading amount [a] (wt%)				Specific surface area ($m^2\ g^{-1}$)	Total pore volume ($cm^3\ g^{-1}$)
	Co[b]	C	N	O		
Pristine graphene		100			1138	0.81
GOOH		43		57	1207	0.62
CoTCPP/GOOH	7 (6.95)	66	7	20	859	0.58
CoTCPP/GOOH [c]	6 (6.95)	68	6	20	232	0.11

[a]Estimated by EDX spectrum as shown in **Figure S1,** in the Supporting Information.

[b]The value in parentheses is the Co loading amount in theory.

[c]After use for the reaction.

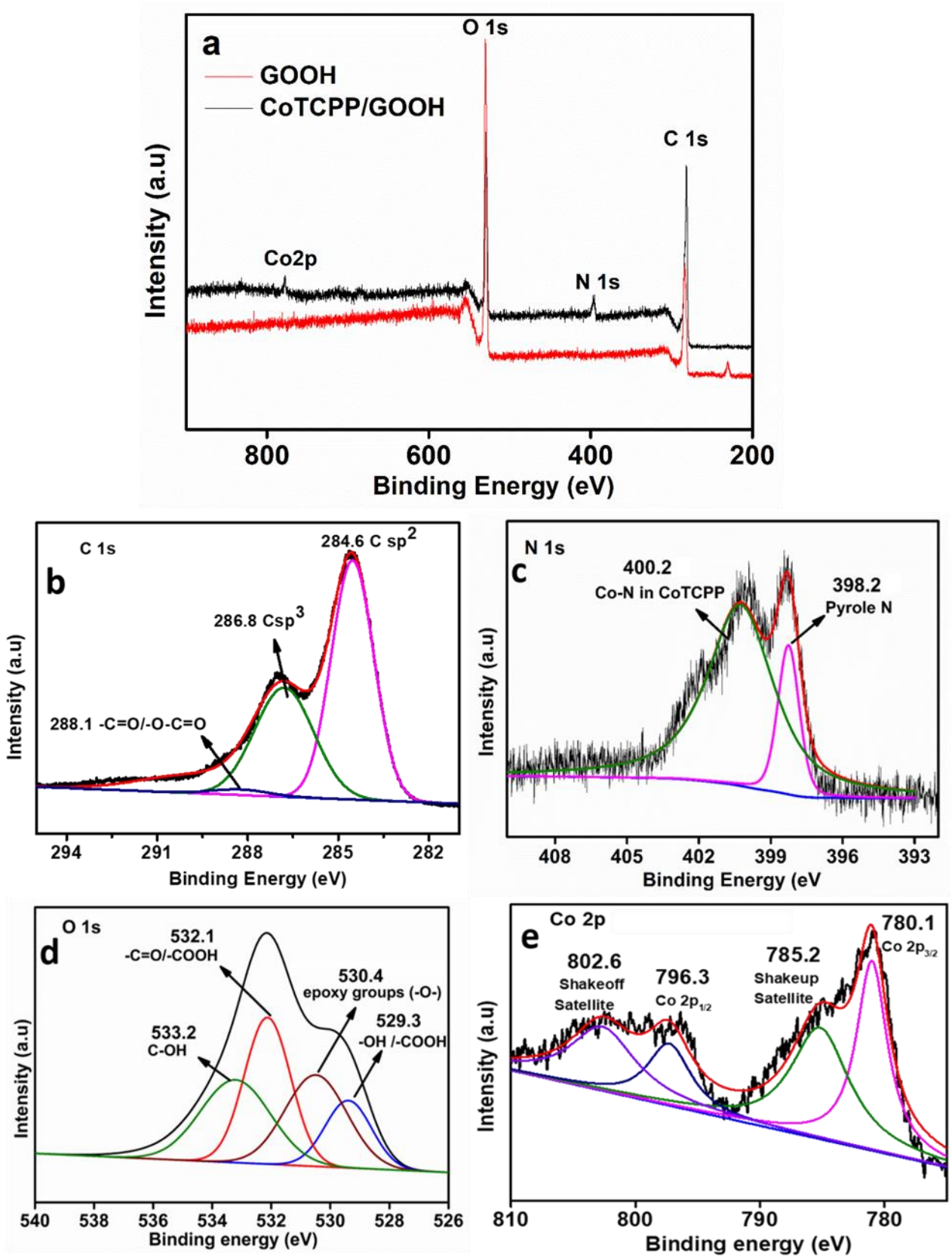

Figure 4. XPS spectra of CoTCPP/GOOH; (a) wide scan, and narrow scans in (b) C 1s, (c) N 1s, (d) O 1s, and (e) Co 2p origin.

Catalytic activity

The thoroughly characterized CoTCPP/GOOH catalyst was used for the liquid-phase oxidation of isoeugenol (**Scheme 2**) to vanillin using molecular oxygen as the oxidant.

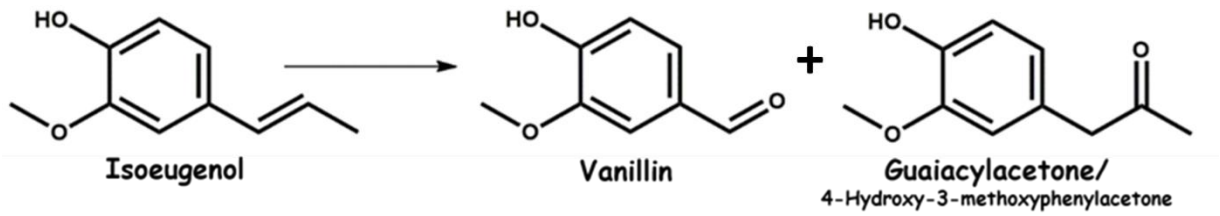

Scheme 2. Isoeugenol oxidation to vanillin over CoTCPP/GOOH catalyst.

The experimental findings revealed the formation of guaiacyl acetone alongside vanillin during the isoeugenol oxidation reaction. A preliminary investigation conducted at 25 °C for 20 h demonstrated a vanillin yield of 38.2% with an isoeugenol conversion of 61.8%. The observed low vanillin yield at lower temperatures is attributed to the formation of unidentified by-products. Previous research also suggested that the diminished vanillin yield could be linked to multiple parallel pathways during isoeugenol oxidation, leading to the generation of various by-products, notably dehydrodiisoeugenol and vanillyl methyl ketone.[30,53] To address this, an increase in reaction temperature from 25 to 100 °C was employed, as shown in **Figure 5**, resulting in a significant enhancement of the vanillin yield, doubling from 38.2% to 75.1% along with the formation of guaiacyl acetone as the by-product. Moreover, extending the reaction time from 1 h to 20 h at 100 °C exhibited a significant increase in vanillin yield from 40.2% to 75.1% (*vide infra*). This observation underscores the importance of prolonged reaction times at elevated temperatures for maximizing vanillin production. Alongside the reaction temperature, the reaction pressure played a crucial role in creating favorable conditions for the efficient conversion of isoeugenol to vanillin. **Figure 6** shows the oxidation of isoeugenol and the product distribution under different pressures ranging from 0.5 to 3.0 MPa. 30.7% of isoeugenol conversion was observed at very low pressures (0.5 MPa) with a vanillin yield of 26.2%. The increase in oxygen pressure from 0.5 to 3.0 MPa led to a sharp increase in the isoeugenol conversion (30.7% to 96.3%) with comparatively good vanillin yield (26.2% to 75.1%). Detailed values for **Figure 5 and 6** are listed in **Table S2** and **S3**, in the Supporting Information.

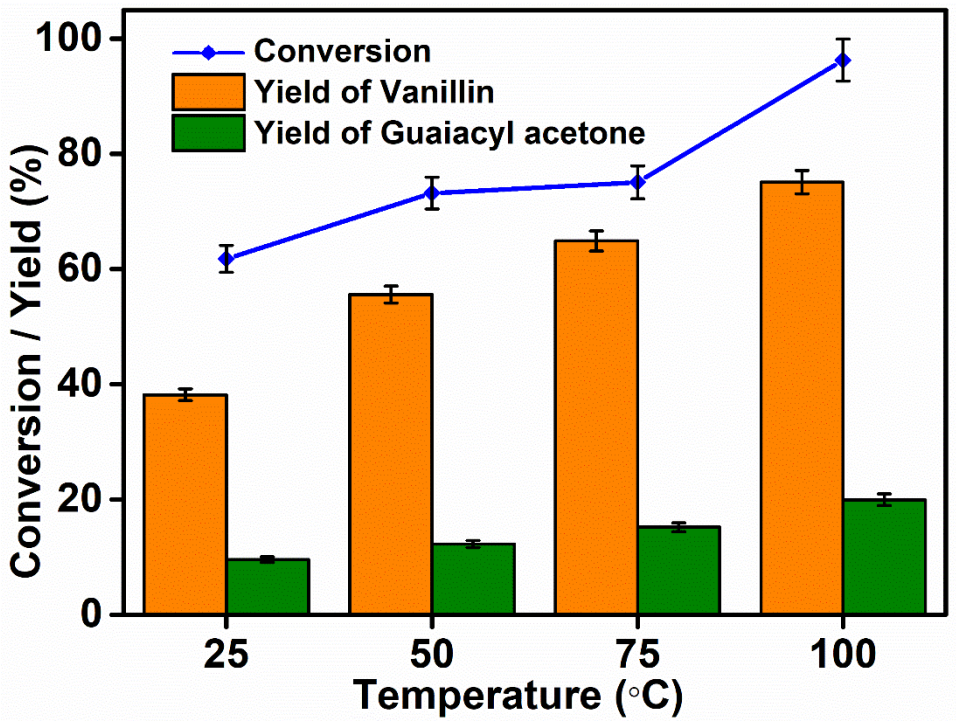

Figure 5. Effect of temperature on isoeugenol oxidation catalyzed by CoTCPP/GOOH. *Reaction condition*: Isoeugenol (1.0 mmol), catalyst (20 mg), Acetonitrile (3.0 mL), 20 h, 3.0 MPa O_2.

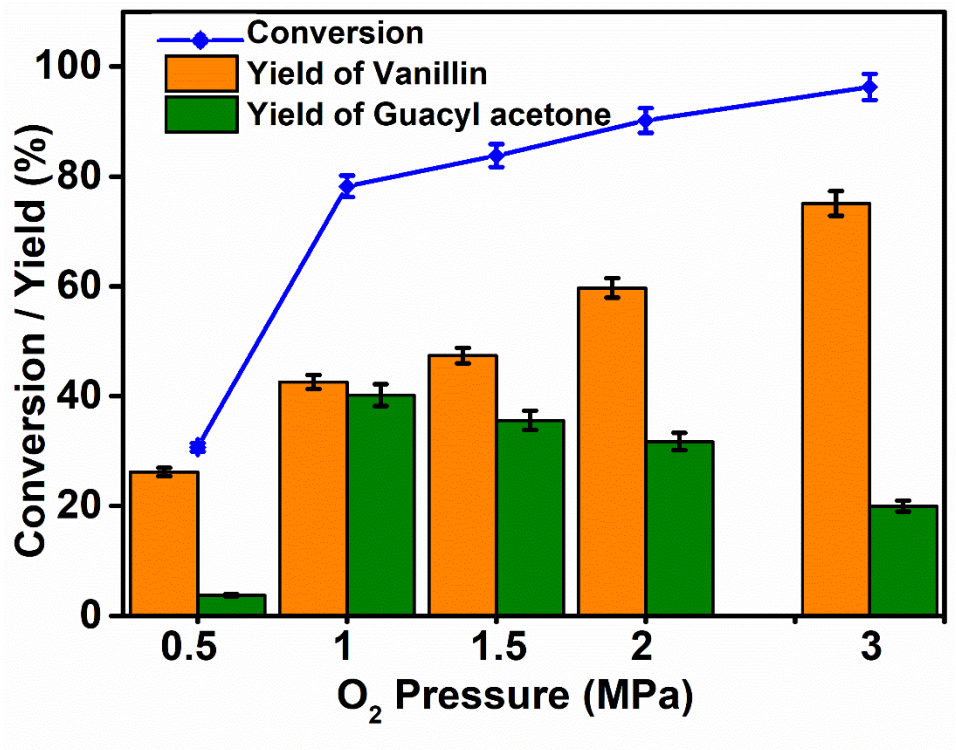

Figure 6. Effect of pressure on isoeugenol oxidation catalyzed by CoTCPP/GOOH. *Reaction condition*: Isoeugenol (1.0 mmol), catalyst (20 mg), Acetonitrile (3.0 mL), 100 °C, 20 h.

Further, we have chosen 100 °C as the reaction temperature and 3.0 MPa as the oxygen pressure, the reaction was followed at different duration. When the reaction time was around 1 h, the isoeugenol conversion was 75.1% with vanillin yield of 40.2%. As the reaction time increased, a steady improvement in the isoeugenol conversion was observed and reached a maximum of 96.1% and a vanillin yield of 75.1% was achieved at 20 h as shown in **Figure 7.** Detailed values are listed in **Table S4**, in the Supporting Information. In addition, we explored the impact of varying catalyst amounts (10 to 100 mg) on the isoeugenol oxidation reaction using CoTCPP/GOOH, while maintaining a constant 1.0 mmol of isoeugenol. Subsequently, the amount of catalyst to be used for the isoeugenol oxidation was further optimized over CoTCPP/GOOH, and then 20 mg of catalyst was found to be the best condition (**Figure S2** and **Table S5**, in the Supporting Information). With a modest catalyst quantity of 10 mg, we observed isoeugenol conversion and vanillin yield at 76.9% and 68.4%, respectively. Increasing the catalyst amount from 10 to 100 mg led to a rise in both isoeugenol conversion and vanillin yield, reaching a peak. However, elevating the catalyst amount beyond 20 mg showed consistent isoeugenol conversion and vanillin yield, around 98.6% to 81.7%, respectively. This suggests that further increases in catalyst amount do not significantly enhance conversion or yield.

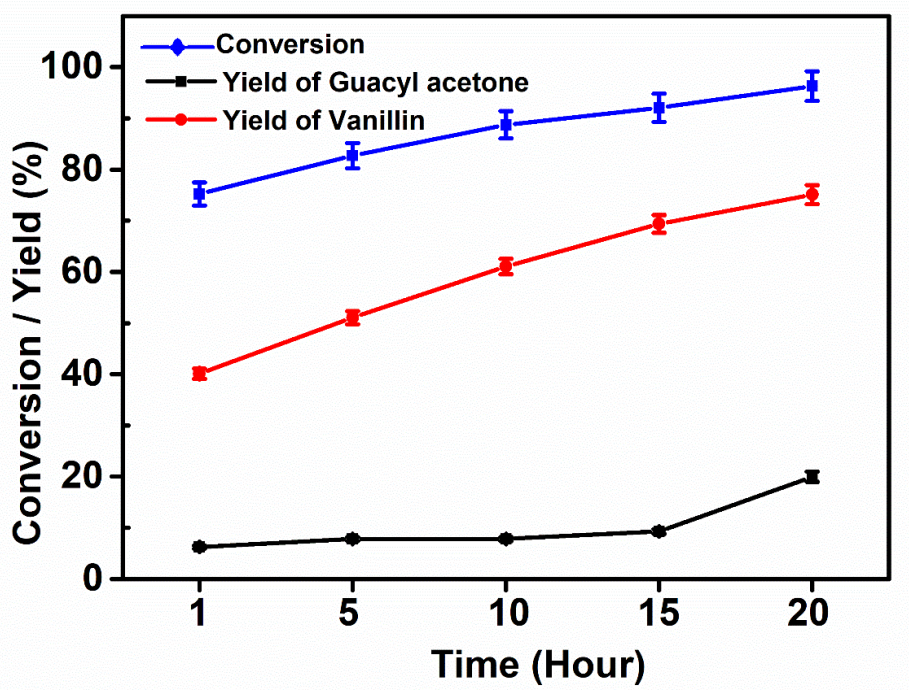

Figure 7. Effect of time on isoeugenol oxidation catalysed by CoTCPP/GOOH. *Reaction condition*: Isoeugenol (1.0 mmol), catalyst (20 mg), Acetonitrile (3.0 mL), 100 °C, 3 MPa O_2.

The stability of the CoTCPP/GOOH catalyst in the isoeugenol oxidation process was systematically assessed, as illustrated in **Figure 8**. Detailed values are listed in **Table S6**, in the Supporting Information. Recyclability testing involved the separation of the catalyst from the reaction mixture through centrifugation, subsequent washing, and overnight drying at 80 °C before initiating the next cycle. Remarkably, the conversion of isoeugenol, exceeding 93%, exhibited consistent performance over five consecutive reaction cycles, underscoring the catalyst's robust stability under the reaction conditions. The enhanced activity observed during the recycle studies is attributed to the immobilization of CoTCPP on the OH-rich graphene oxide. We also conducted a gram-scale experiment with 10 mmol of isoeugenol (1.64 g) to check the scalability of the process. After 48 h of reaction at 100 °C, it shows almost 93% isoeugenol conversion with 72% yield of vanillin, demonstrating the scalability of the process.

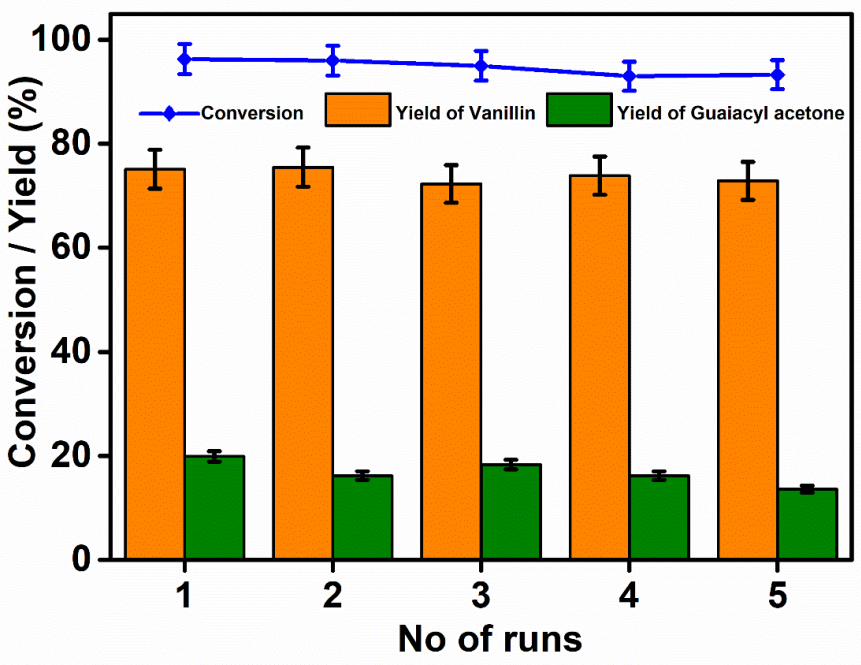

Figure 8. Recyclability of CoTCPP/GOOH. *Reaction condition*: Isoeugenol (1.0 mmol), catalyst (20 mg), Acetonitrile (3.0 mL), O_2 (3.0 MPa), 100 °C, 20 h.

To elucidate the role of the solvent, we further investigated the reaction using various solvents, with summarized results in **Figure S4** and **Table S7**, in the Supporting Information. Notably, acetonitrile demonstrated outstanding conversion (96.3%) and vanillin yield (75.1%) compared to other solvents. Nonpolar solvents like cyclohexanone and cyclohexane exhibited lower efficiency, likely due to their reduced ability to solubilize reactants, catalysts, and molecular oxygen. Acetonitrile, characterized by high polarity and a substantial dielectric constant, facilitated superior solubility of both reactants and catalysts. The polar nature of

acetonitrile additionally contributed to increased reactivity and improved catalyst accessibility to reactants. While ethanol and methanol also possess polar characteristics, their lower dielectric constants compared to acetonitrile resulted in comparatively reduced solubility of reactants and catalysts.[54,55] This limitation in solubility may influence the reaction rate, consequently lowering overall conversion when compared with acetonitrile.

To ascertain the absence of homogeneous catalysis, a hot filtration test was conducted on the model reaction. Following a 5 h reaction period, the catalyst underwent a hot filtration and subsequent analysis, revealing a conversion rate of approximately 83% and a yield of 51% for vanillin. Subsequently, the filtrate underwent an additional 15 h reaction period, during which the conversion rate and product yield remained relatively stable. Furthermore, a heterogeneity test was performed using the catalyst poison QuadraPure®TU. To ensure complete binding of all Co species present in the reaction mixture, QuadraPure®TU was utilized at a concentration four times higher than the established scavenging limit of 0.19 mmol Co per gram of QuadraPure®TU.[56] As a control, CoTCPP (0.06 mmol; containing 0.0169 mmol Co) was employed as the catalyst in conjunction with twice the necessary amount of QuadraPure®TU to bind all cobalt present in the reaction mixture. Experimental findings indicate that the inclusion of up to four equivalents of QuadraPure®TU had no significant effect on the catalytic activity of CoTCPP/GOOH in the isoeugenol oxidation reaction. Notably, the catalytic system maintained a high conversion rate exceeding 95% and a yield of 75% for the desired product, underscoring the robustness and heterogeneous nature of the CoTCPP/GOOH catalyst. Conversely, the control experiment utilizing CoTCPP and two equivalents of QuadraPure®TU resulted in negligible product formation, with only 9% isoeugenol conversion and unidentified products. This observation confirms the absence of homogeneous CoTCPP species catalysing the isougenol oxidation under optimized reaction conditions, further supporting the heterogeneous nature of the CoTCPP/GOOH catalyst. Moreover, analysis via SEM-EDS revealed that the structure of the heterogenized catalyst remained unaltered post-reaction. The SEM-EDX data indicated no significant decrease in the weight percentage of Co, with a slight increase in carbon content observed in the CoTCPP/GOOH catalyst: fresh (Co: 6 wt%, C: 66 wt%) and used (Co: 6 wt%, C: 68 wt%), as listed in **Table 1**. Additionally, the specific surface area of the used catalyst decreased to 232 $m^2 g^{-1}$ from 859 $m^2 g^{-1}$ for the fresh catalyst. This phenomenon could potentially be attributed to the deposition or chemisorption of reactant molecules onto the catalyst surface.

Further, to calculate the activation energy, the kinetic study was performed under different temperatures (ranging from 313 to 373 K) and times (from 30 to 120 min) using 1.0 mmol of isoeugenol as the substrate, and the results are depicted in **Figure 9.** The initial rates were calculated at different temperatures (as listed in **Table S8**, in the Supporting Information) and Arrhenius plots of ln (initial rate) vs. 1/T were made (**Figure 10**) at 30 min. The apparent activation energy for the reaction was calculated from the slope as 21.58 kJ mol^{-1} which is comparable to that of literature reports, 24.63 kJ mol^{-1}.[57] The high values of apparent activation energy confirm that the reaction system was kinetically controlled.

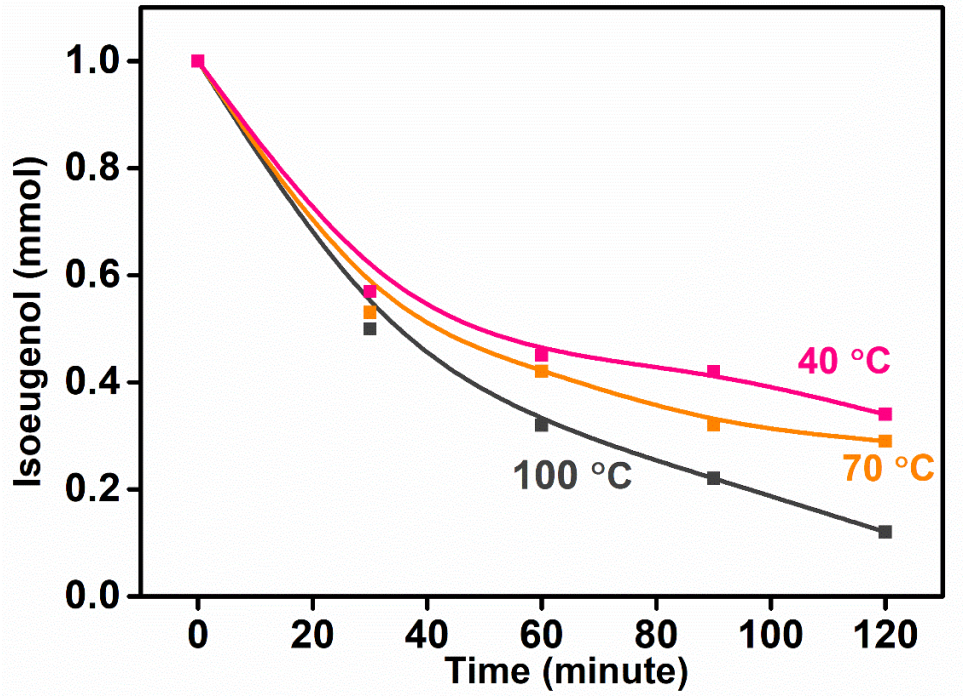

Figure 9. Isoeugenol concentration profiles at 40, 70 and 100 °C. *Reaction conditions*: Isoeugenol (1.0 mmol), catalyst (20 mg), acetonitrile (3.0 mL), and 3.0 MPa O_2 pressure.

Further to determine the order of reaction with respect to the concentration of reactant, isoeugenol the initial reaction rate was calculated at different isoeugenol concentrations (0.25, 0.5, 1.0, 1.5, 2.0, and 3.0 mmol) at 30 min. A plot of ln (initial rate) against ln (Initial isoeugenol concentration) was made and shown in **Figure 11a**. From the slope of the linear fit line, the order of reaction was determined. The order of the reaction was found to be 1 with respect to the isoeugenol concentration. In addition, the order of the reaction with respect to the oxygen pressure was calculated as shown in **Figure 11b** and obtained as 0.5. Further, the effect of catalyst concentration was studied and a plot of ln (initial rate) against ln (amount of Catalyst, CoTCPP/GOOH) was made as shown in **Figure 11c**. From the slope of the linear fit line, the

order of the reaction with respect to catalysts was determined and was found to be 0. So, the overall order of the reaction was the sum of the order with respect to the concentration of isoeugenol, catalyst, and oxygen pressure and it was about 3/2 hence the rate equation can be written as

$$\text{Rate} = K\,[\text{Isoeugenol}]^{1}[O_2]^{1/2}$$

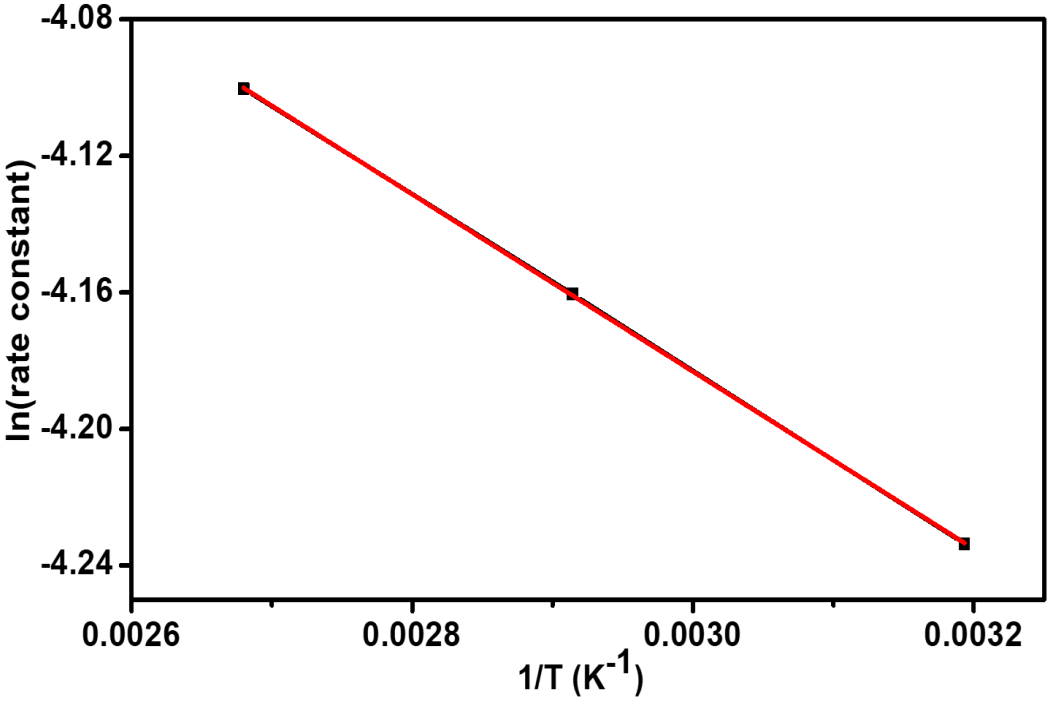

Figure 10. Arrhenius plot (plot of ln (initial rate) vs. 1/T). *Reaction conditions*: Isoeugenol (1 mmol), catalyst (20 mg), acetonitrile (3.0 mL), and 3.0 MPa O_2 pressure, 30 min.

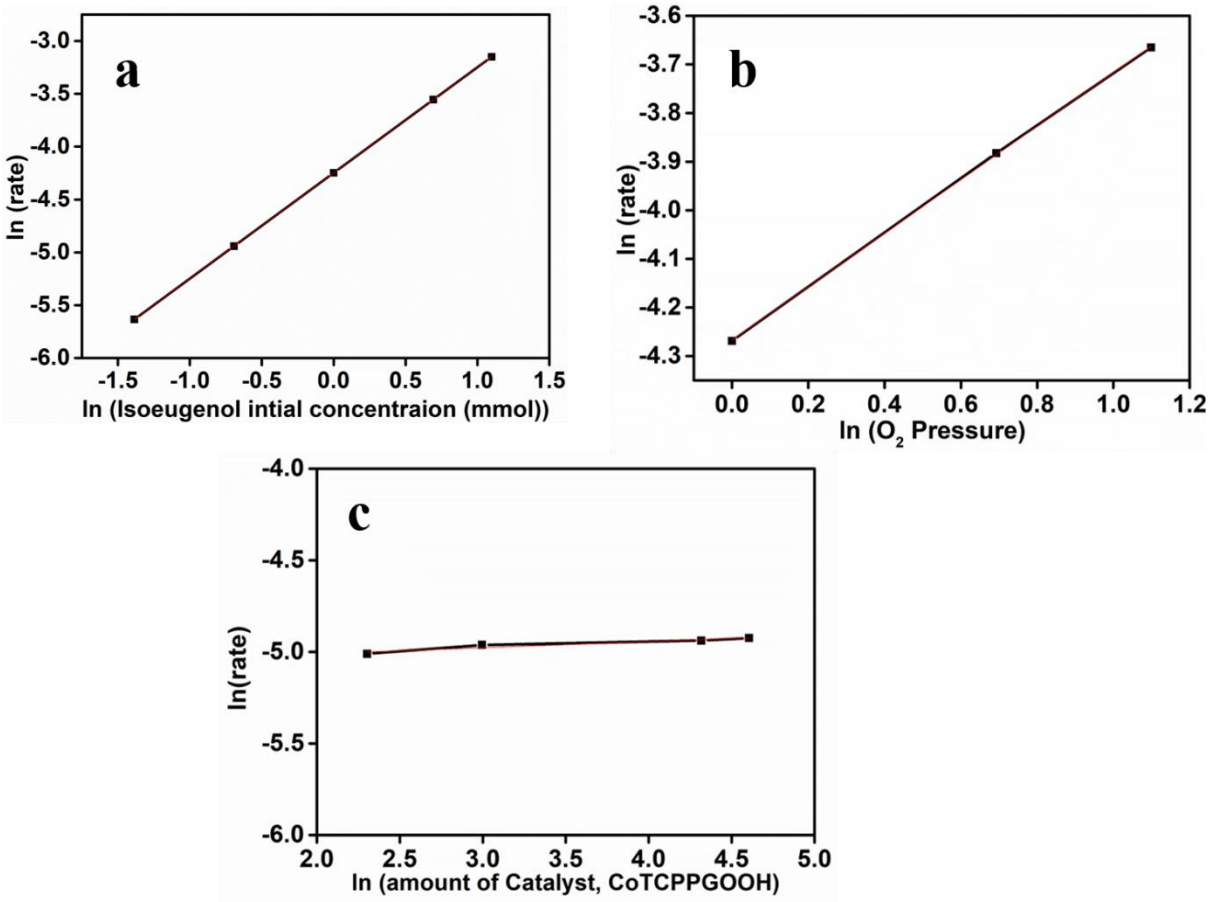

Figure 11. Plot of ln (rate) vs. (a) ln (Isoeugenol concentration in mmol), (b) ln (O_2 pressure in MPa), (c) ln (amount of catalysts, CoTCPPGOOH in mg).

Regarding the reaction mechanism, previous studies have emphasised the pivotal role of Co–salen complexes in mediating the oxidative cleavage of isoeugenol. This process initiates with an attack by a Co-O_2 species at the allyl substituent, subsequently leading to the formation of vanillin.[31] Concurrently, the anti-Markovnikov oxidation pathway results in the generation of guaiacyl acetone as a by-product.[58] Our recent investigation, also supports these findings, highlights the analogous mechanism facilitated by the Co-porphyrin system. Activation of molecular oxygen by the Co-porphyrin system and the formation of a superoxide species, which, similar to its Co–salen counterpart, activates the allyl group of isoeugenol, ultimately yielding vanillin.[59] Moreover, the anti-Markovnikov oxidation pathway gives rise to guaiacyl acetone as an accompanying by-product. These findings collectively contribute to a comprehensive understanding of the mechanism involved in the catalytic cleavage of isoeugenol.

CONCLUSION

In conclusion, this study presents a novel approach involving the immobilization of isolated CoTCPP onto a hydroxyl-rich graphene oxide (GOOH) support, resulting in the synthesis of CoTCPP/GOOH. The catalyst exhibited remarkable efficiency in the oxidative cleavage of biomass-derived isoeugenol to vanillin, highlighting its potential in sustainable catalytic applications. Through comprehensive experimental characterization, including FT-IR, XRD, BET surface area analysis, SEM-EDX elemental mapping, and XPS spectroscopy, the successful grafting of cobalt-porphyrin onto the GOOH surface was confirmed, elucidating the structural and chemical attributes of the catalyst. Further the catalytic activity of CoTCPP/GOOH was systematically evaluated in the oxidation of isoeugenol, demonstrating notable performance enhancements with variations in reaction parameters such as temperature, pressure, reaction time, and catalyst loading. Notably, the catalyst exhibited robust stability over multiple reaction cycles. The kinetic studies revealed valuable insights into the reaction mechanism, elucidating the order of reaction with respect to isoeugenol concentration, oxygen pressure, and catalyst concentration. The observed overall reaction order of 3/2 corroborates the proposed rate equation, indicating a first-order dependence on isoeugenol concentration and a square-root dependence on oxygen pressure. Furthermore, the mechanistic investigation aligns with previous studies, emphasizing the critical role of cobalt-porphyrin complexes in mediating the oxidative cleavage of isoeugenol. The proposed mechanism involves the activation of molecular oxygen by the Co-porphyrin system, leading to the formation of a superoxide species. This species initiates the attack at the allyl group of isoeugenol, yielding vanillin, with guaiacyl acetone formed as a by-product via the anti-Markovnikov oxidation pathway.

ASSOCIATEDCONTENT

*SI Supporting Information

The Supporting Information is available free of charge at XXXXXXXXXXXXX.

Materials, SEM-EDS spectra, and kinetics study tables.

AUTHOR INFORMATION

Corresponding Author

Kaiprathu Anjali

Graduate School of Advanced Science and Technology, Japan Advanced Institute of Science and Technology, 1-1 Asahidai, Nomi, Ishikawa 923-1292, Japan. Email: anjali@jaist.ac.jp

Shun Nishimura

Graduate School of Advanced Science and Technology, Japan Advanced Institute of Science and Technology, 1-1 Asahidai, Nomi, Ishikawa 923-1292, Japan.

Research Center for Carbon Neutral, Japan Advanced Institute of Science and Technology, 1-1 Asahidai, Nomi, Ishikawa 923-1292, Japan, Email: s_nishim@jaist.ac.jp

Notes

The authors declare no competing financial interest.

ACKNOWLEDGMENTS

This research has been generously supported by the Japan Society for the Promotion of Science (JSPS) for the Grant-in-Aid for JSPS Fellows (KAKENHI, No.22F32039). KA is grateful to the JSPS postdoctoral fellowships for research in Japan.

REFERENCE

(1) Gollakota, A. R. K.; Shu, C.-M.; Sarangi, P. K.; Shadangi, K. P.; Rakshit, S.; Kennedy, J. F.; Gupta, V. K.; Sharma, M. Catalytic Hydrodeoxygenation of Bio-Oil and Model Compounds - Choice of Catalysts, and Mechanisms. *Renew. Sustain. Energy Rev.* **2023**, *187*, 113700. https://doi.org/https://doi.org/10.1016/j.rser.2023.113700.

(2) Singh, K.; Mehra, S.; Kumar, A. Recent Advances in Catalytic Conversion of Lignin to Value-Added Chemicals Using Ionic Liquids and Deep Eutectic Solvents: A Critical Review. *Green Chem.* **2024**, *26* (3), 1062–1091. https://doi.org/10.1039/D3GC03439A.

(3) Faizan, M.; Song, H. Critical Review on Catalytic Biomass Gasification: State-of-Art Progress, Technical Challenges, and Perspectives in Future Development. *J. Clean. Prod.* **2023**, *408*, 137224. https://doi.org/https://doi.org/10.1016/j.jclepro.2023.137224.

(4) Güleç, F.; Parthiban, A.; Umenweke, G. C.; Musa, U.; Williams, O.; Mortezaei, Y.; Suk-Oh, H.; Lester, E.; Ogbaga, C. C.; Gunes, B.; Okolie, J. A. Progress in Lignocellulosic Biomass Valorization for Biofuels and Value-Added Chemical

Production in the EU: A Focus on Thermochemical Conversion Processes. *Biofuels, Bioprod. Biorefining* **2023**, 1–27. https://doi.org/10.1002/bbb.2544.

(5) Peters, M. A.; Alves, C. T.; Onwudili, J. A. A Review of Current and Emerging Production Technologies for Biomass-Derived Sustainable Aviation Fuels. *Energies* **2023**, *16* (16). https://doi.org/10.3390/en16166100.

(6) Quevedo, R. A.; Blanca, A.; Escalera, P.; Aida, V.; Arias, M. R.; Reynel, H. E.; Moreno, J. C.; Liliana, P.; Bonilla, G. A. *Application of Waste Biomass for the Production of Biofuels and Catalysts : A Review*; Springer Berlin Heidelberg, 2024. https://doi.org/10.1007/s10098-023-02728-4.

(7) Rodríguez-Padrón, D.; Puente-Santiago, A. R.; Balu, A. M.; Muñoz-Batista, M. J.; Luque, R. Environmental Catalysis: Present and Future. *ChemCatChem* **2019**, *11* (1), 18–38. https://doi.org/10.1002/cctc.201801248.

(8) Ravi, K. Catalyst Development for Biomass Conversion to Fuel and High Value Added Chemicals Dedicated to Rural Children. **2023**, No. June.

(9) Wang, A.; Austin, D.; Song, H. Investigations of Thermochemical Upgrading of Biomass and Its Model Compounds: Opportunities for Methane Utilization. *Fuel* **2019**, *246* (January), 443–453. https://doi.org/10.1016/j.fuel.2019.03.015.

(10) Franco, A.; Fernandes De Souza, J.; Pinheiro Do Nascimiento, P. F.; Mendes Pedroza, M.; De Carvalho, L. S.; Rodriguez-Castellón, E.; Luque, R. Sewage Sludge-Derived Materials as Efficient Catalysts for the Selective Production of Vanillin from Isoeugenol. *ACS Sustain. Chem. Eng.* **2019**, *7* (8), 7519–7526. https://doi.org/10.1021/acssuschemeng.8b05105.

(11) Bhavisha, M.; Aswani, S.; Sreenavya, A.; Neethu, P. P.; Archana, I. G.; Balamurugan, S.; Ganesh, V.; Sakthivel, A. Molybdenum Incorporated Strontium-Iron and Strontium-Cobalt (SrBMoO3−δ; B=Fe & Co) Perovskites: Preparation and Their Application on Oxidation of Iso-Eugenol into Vanillin. *Eur. J. Inorg. Chem.* **2023**, *26* (3). https://doi.org/10.1002/ejic.202200590.

(12) Neethu, P. P.; Sreenavya, A.; Sakthivel, A. Molybdate Stabilized Magnesium-Iron Hydrotalcite Materials: Potential Catalysts for Isoeugenol to Vanillin and Olefin Epoxidation. *Appl. Catal. A Gen.* **2021**, *623* (April).

https://doi.org/10.1016/j.apcata.2021.118292.

(13) Sahu, P.; Tincy, A.; Sreenavya, A.; Shanbhag, G.; Sakthivel, A. Molybdenum Carbonyl Grafted on Amine-Functionalized MCM-22 as Potential Catalyst for Iso-Eugenol Oxidation. *Catal. Letters* **2021**, *151* (5), 1336–1349. https://doi.org/10.1007/s10562-020-03388-5.

(14) Cañadas, R.; González-Miquel, M.; González, E. J.; Núñez De Prado, A.; Díaz, I.; Rodríguez, M. Sustainable Recovery of High Added-Value Vanilla Compounds from Wastewater Using Green Solvents. *ACS Sustain. Chem. Eng.* **2021**, *9* (13), 4850–4862. https://doi.org/10.1021/acssuschemeng.1c00168.

(15) D'Arrigo, P.; Rossato, L. A. M.; Strini, A.; Serra, S. From Waste to Value: Recent Insights into Producing Vanillin from Lignin. *Molecules* **2024**, *29* (2), 1–32. https://doi.org/10.3390/molecules29020442.

(16) Galadima, A. I.; Salleh, M. M.; Hussin, H.; Chong, C. S.; Yahya, A.; Mohamad, S. E.; Abd-Aziz, S.; Yusof, N. N. M.; Naser, M. A.; Al-Junid, A. F. M. Biovanillin: Production Concepts and Prevention of Side Product Formation. *Biomass Convers. Biorefinery* **2020**, *10* (2), 589–609. https://doi.org/10.1007/s13399-019-00418-0.

(17) Xu, L.; Liaqat, F.; Sun, J.; Khazi, M. I.; Xie, R.; Zhu, D. Advances in the Vanillin Synthesis and Biotransformation: A Review. *Renew. Sustain. Energy Rev.* **2024**, *189* (PA), 113905. https://doi.org/10.1016/j.rser.2023.113905.

(18) Rao, S. R.; Ravishankar, G. A. Vanilla Flavour: Production by Conventional and Biotechnological Routes. *J. Sci. Food Agric.* **2000**, *80* (3), 289–304. https://doi.org/10.1002/1097-0010(200002)80:3<289::aid-jsfa543>3.0.co;2-2.

(19) Sharma, A.; Sahu, S.; Sharma, S.; Singh, G.; Arya, S. K. Valorization of Agro-Industrial Wastes into Vanillin: A Sustainable and Bio-Economical Step towards the Indigenous Production of Flavors. *Biocatal. Agric. Biotechnol.* **2023**, *54* (July), 102904. https://doi.org/10.1016/j.bcab.2023.102904.

(20) Lai, H.; Zhang, J.; Xiao, P. Renewable Photopolymers: Transformation of Biomass Resources into Value-Added Products Under Light. *ACS Sustain. Chem. Eng.* **2023**, *11* (46), 16365–16406. https://doi.org/10.1021/acssuschemeng.3c05257.

(21) Shinde, S. H.; Hengne, A.; Rode, C. V. Chapter 1 - Lignocellulose-Derived Platform

Molecules: An Introduction. In *Biomass, Biofuels, Biochemicals*; Saravanamurugan, S., Pandey, A., Li, H., Riisager, A., Eds.; Biomass, Biofuels, Biochemicals; Elsevier, 2020; pp 1–31. https://doi.org/https://doi.org/10.1016/B978-0-444-64307-0.00001-9.

(22) Wan Mahari, W. A.; Waiho, K.; Fazhan, H.; Necibi, M. C.; Hafsa, J.; Mrid, R. Ben; Fal, S.; El Arroussi, H.; Peng, W.; Tabatabaei, M.; Aghbashlo, M.; Almomani, F.; Lam, S. S.; Sillanpää, M. Progress in Valorisation of Agriculture, Aquaculture and Shellfish Biomass into Biochemicals and Biomaterials towards Sustainable Bioeconomy. *Chemosphere* **2022**, *291* (August 2021). https://doi.org/10.1016/j.chemosphere.2021.133036.

(23) Martău, G. A.; Călinoiu, L. F.; Vodnar, D. C. Bio-Vanillin: Towards a Sustainable Industrial Production. *Trends Food Sci. Technol.* **2021**, *109* (January), 579–592. https://doi.org/10.1016/j.tifs.2021.01.059.

(24) Ciriminna, R.; Fidalgo, A.; Meneguzzo, F.; Parrino, F.; Ilharco, L. M.; Pagliaro, M. Vanillin: The Case for Greener Production Driven by Sustainability Megatrend. *ChemistryOpen* **2019**, *8* (6), 660–667. https://doi.org/10.1002/open.201900083.

(25) Khalil, A. A.; Rahman, U. U.; Khan, M. R.; Sahar, A.; Mehmood, T.; Khan, M. Essential Oil Eugenol: Sources, Extraction Techniques and Nutraceutical Perspectives. *RSC Adv.* **2017**, *7* (52), 32669–32681. https://doi.org/10.1039/c7ra04803c.

(26) Liu, Y.; Sun, L.; Huo, Y. X.; Guo, S. Strategies for Improving the Production of Bio-Based Vanillin. *Microb. Cell Fact.* **2023**, *22* (1), 1–11. https://doi.org/10.1186/s12934-023-02144-9.

(27) Di Paola, A.; Bellardita, M.; Megna, B.; Parrino, F.; Palmisano, L. Photocatalytic Oxidation of Trans-Ferulic Acid to Vanillin on TiO2 and WO3-Loaded TiO2 Catalysts. *Catal. Today* **2015**, *252*, 195–200. https://doi.org/10.1016/j.cattod.2014.09.012.

(28) Jiang, J.-A.; Chen, C.; Guo, Y.; Liao, D.-H.; Pan, X.-D.; Ji, Y.-F. A Highly Efficient Approach to Vanillin Starting from 4-Cresol. *Green Chem.* **2014**, *16* (5), 2807–2814. https://doi.org/10.1039/C4GC00003J.

(29) Delisi, R.; Ciriminna, R.; Parrino, F.; Palmisano, L.; Xu, Y. J.; Pagliaro, M. One-Pot, Clean Synthesis of Vanillic Acid from Ferulic Acid. *ChemistrySelect* **2016**, *1* (3), 626–

629. https://doi.org/10.1002/slct.201600111.

(30) Gusevskaya, E. V.; Menini, L.; Parreira, L. A.; Mesquita, R. A.; Kozlov, Y. N.; Shul'Pin, G. B. Oxidation of Isoeugenol to Vanillin by the "h 2O 2-Vanadate-Pyrazine-2-Carboxylic Acid" Reagent. *J. Mol. Catal. A Chem.* **2012**, *363–364*, 140–147. https://doi.org/10.1016/j.molcata.2012.06.001.

(31) Adilina, I. B.; Hara, T.; Ichikuni, N.; Shimazu, S. Oxidative Cleavage of Isoeugenol to Vanillin under Molecular Oxygen Catalysed by Cobalt Porphyrin Intercalated into Lithium Taeniolite Clay. *J. Mol. Catal. A Chem.* **2012**, *361–362*, 72–79. https://doi.org/10.1016/j.molcata.2012.05.005.

(32) Meunier, B. Metalloporphyrins as Versatile Catalysts for Oxidation Reactions and Oxidative DNA Cleavage. *Chem. Rev.* **1992**, *92* (6), 1411–1456. https://doi.org/10.1021/cr00014a008.

(33) Mansuy, D. A Brief History of the Contribution of Metalloporphyrin Models to Cytochrome P450 Chemistry and Oxidation Catalysis. *Comptes Rendus Chim.* **2007**, *10* (4–5), 392–413. https://doi.org/10.1016/j.crci.2006.11.001.

(34) Wang, D.; Groves, J. T. Efficient Water Oxidation Catalyzed by Homogeneous Cationic Cobalt Porphyrins with Critical Roles for the Buffer Base. *Proc. Natl. Acad. Sci. U. S. A.* **2013**, *110* (39), 15579–15584. https://doi.org/10.1073/pnas.1315383110.

(35) Pamin, K.; Tabor, E.; Górecka, S.; Kubiak, W. W.; Rutkowska-Zbik, D.; Połtowicz, J. Three Generations of Cobalt Porphyrins as Catalysts in the Oxidation of Cycloalkanes. *ChemSusChem* **2019**, *12* (3), 684–691. https://doi.org/10.1002/cssc.201802198.

(36) Bedioui, F. Zeolite-Encapsulated and Clay-Intercalated Metal Porphyrin, Phthalocyanine and Schiff-Base Complexes as Models for Biomimetic Oxidation Catalysts: An Overview. *Coord. Chem. Rev.* **1995**, *144*, 39–68. https://doi.org/https://doi.org/10.1016/0010-8545(94)08000-H.

(37) Takagi, S.; Eguchi, M.; Tryk, D. A.; Inoue, H. Porphyrin Photochemistry in Inorganic/Organic Hybrid Materials: Clays, Layered Semiconductors, Nanotubes, and Mesoporous Materials. *J. Photochem. Photobiol. C Photochem. Rev.* **2006**, *7* (2–3), 104–126. https://doi.org/10.1016/j.jphotochemrev.2006.04.002.

(38) Zyoud, A.; Jondi, W.; Mansour, W.; Majeed Khan, M. A.; Hilal, H. S. Modes of

Tetra(4-Pyridyl)Porphyrinatomanganese(III) Ion Intercalation inside Natural Clays. *Chem. Cent. J.* **2016**, *10* (1), 1–9. https://doi.org/10.1186/s13065-016-0153-4.

(39) Peng, W.; Liu, S.; Sun, H.; Yao, Y.; Zhi, L.; Wang, S. Synthesis of Porous Reduced Graphene Oxide as Metal-Free Carbon for Adsorption and Catalytic Oxidation of Organics in Water. *J. Mater. Chem. A* **2013**, *1* (19), 5854–5859. https://doi.org/10.1039/C3TA10592J.

(40) Mombeshora, E. T.; Stark, A. Graphene Oxide Applications in Biorefinery Catalysis to Chemical Commodities: Critical Review, Prospects and Challenges. *Biomass Convers. Biorefinery* **2023**, *13* (6), 4619–4638. https://doi.org/10.1007/s13399-021-01499-6.

(41) Fakhri, P.; Jaleh, B.; Nasrollahzadeh, M. Synthesis and Characterization of Copper Nanoparticles Supported on Reduced Graphene Oxide as a Highly Active and Recyclable Catalyst for the Synthesis of Formamides and Primary Amines. *J. Mol. Catal. A Chem.* **2014**, *383–384*, 17–22. https://doi.org/10.1016/j.molcata.2013.10.027.

(42) Anjali, K.; Nishimura, S. Efficient Conversion of Furfural to Succinic Acid Using Cobalt-Porphyrin Based Catalysts and Molecular Oxygen. *J. Catal.* **2023**, *428* (August), 115182. https://doi.org/10.1016/j.jcat.2023.115182.

(43) Chen, J.; Zhang, Y.; Zhang, M.; Yao, B.; Li, Y.; Huang, L.; Li, C.; Shi, G. Water-Enhanced Oxidation of Graphite to Graphene Oxide with Controlled Species of Oxygenated Groups. *Chem. Sci.* **2016**, *7* (3), 1874–1881. https://doi.org/10.1039/c5sc03828f.

(44) Rayati, S.; Nejabat, F. The Catalytic Efficiency of Fe-Porphyrins Supported on Multi-Walled Carbon Nanotubes in the Oxidation of Olefins and Sulfides with Molecular Oxygen. *New J. Chem.* **2017**, *41* (16), 7987–7991. https://doi.org/10.1039/c7nj01530e.

(45) Rayati, S.; Nejabat, F. Catalytic Activity of Fe-Porphyrins Grafted on Multiwalled Carbon Nanotubes in the Heterogeneous Oxidation of Sulfides and Degradation of Phenols in Water. *Comptes Rendus Chim.* **2017**, *20* (9–10), 967–974. https://doi.org/10.1016/j.crci.2017.05.004.

(46) Sonkar, P. K.; Prakash, K.; Yadav, M.; Ganesan, V.; Sankar, M.; Gupta, R.; Yadav, D. K. Co(II)-Porphyrin-Decorated Carbon Nanotubes as Catalysts for Oxygen Reduction Reactions: An Approach for Fuel Cell Improvement. *J. Mater. Chem. A* **2017**, *5* (13),

6263–6276. https://doi.org/10.1039/c6ta10482g.

(47) Ghadamyari, Z.; Khojastehnezhad, A.; Seyedi, S. M.; Shiri, A. Co(II)-Porphyrin Immobilized on Graphene Oxide: An Efficient Catalyst for the Beckmann Rearrangement. *ChemistrySelect* **2019**, *4* (36), 10920–10927. https://doi.org/10.1002/slct.201902811.

(48) Barraza Alvarez, I.; Wu, Y.; Sanchez, J.; Ge, Y.; Ramos-Garcés, M. V.; Chu, T.; Jaramillo, T. F.; Colón, J. L.; Villagrán, D. Cobalt Porphyrin Intercalation into Zirconium Phosphate Layers for Electrochemical Water Oxidation. *Sustain. Energy Fuels* **2021**, *5* (2), 430–437. https://doi.org/10.1039/d0se01134g.

(49) Yuan, Q.; Xing, Y.; Borguet, E. An STM Study of the PH Dependent Redox Activity of a Two-Dimensional Hydrogen Bonding Porphyrin Network at an Electrochemical Interface. *J. Am. Chem. Soc.* **2010**, *132* (14), 5054–5060. https://doi.org/10.1021/ja907397u.

(50) Diskin-Posner, Y.; Goldberg, I. From Porphyrin Sponges to Porphyrin Sieves: A Unique Crystalline Lattice of Aquazinc Tetra(4-Carboxyphenyl)Porphyrin with Nanosized Channels. *Chem. Commun.* **1999**, No. 19, 1961–1962. https://doi.org/10.1039/a906085e.

(51) Li, N.; Lu, W.; Pei, K.; Chen, W. Interfacial Peroxidase-like Catalytic Activity of Surface-Immobilized Cobalt Phthalocyanine on Multiwall Carbon Nanotubes. *RSC Adv.* **2015**, *5* (13), 9374–9380. https://doi.org/10.1039/c4ra15306e.

(52) Zuo, Q.; Cheng, G.; Luo, W. A Reduced Graphene Oxide/Covalent Cobalt Porphyrin Framework for Efficient Oxygen Reduction Reaction. *Dalt. Trans.* **2017**, *46* (29), 9344–9348. https://doi.org/10.1039/c7dt01694h.

(53) Bohre, A.; Gupta, D.; Alam, M. I.; Sharma, R. K.; Saha, B. Aerobic Oxidation of Isoeugenol to Vanillin with Copper Oxide Doped Reduced Graphene Oxide. *ChemistrySelect* **2017**, *2* (10), 3129–3136. https://doi.org/10.1002/slct.201700415.

(54) Zielinski, M.; Samokhvalov, A.; Roche, A. J. Photocatalytic and Photochemical Reactions of Naturally Occurring Phenolic Compounds of Lignin Origin. **2013**, No. May 2013.

(55) Jana, N. C.; Sethi, S.; Saha, R.; Bagh, B. Aerobic Oxidation of Vanillyl Alcohol to

Vanillin Catalyzed by Air-Stable and Recyclable Copper Complex and TEMPO under Base-Free Conditions. *Green Chem.* **2022**, *24* (6), 2542–2556. https://doi.org/10.1039/D1GC04690J.

(56) Choudhary, H.; Nishimura, S.; Ebitani, K. Tailored Design of Palladium Species Grafted on an Amino Functionalized Organozinc Coordination Polymer as a Highly Pertinent Heterogeneous Catalyst. *J. Mater. Chem. A* **2014**, *2* (43), 18687–18696. https://doi.org/10.1039/C4TA03889D.

(57) Prabhu, D. V.; Tandel, M. A.; Parbat, H. A. Kinetic and Thermodynamic Studies of the Oxidation of Eugenol and Isoeugenol by Sodium N-Chlorobenzene-p-Sulphonamide in NaOH. *Asian J. Chem.* **2011**, *23* (12), 5503–5505.

(58) Filiciotto, L.; Márquez-Medina, M. D.; Pineda, A.; Balu, A. M.; Romero, A. A.; Angelici, C.; de Jong, E.; van der Waal, J. C.; Luque, R. Continuous Flow Study of Isoeugenol to Vanillin: A Bio-Based Iron Oxide Catalyst. *Catal. Today* **2021**, *368* (September 2019), 281–290. https://doi.org/10.1016/j.cattod.2019.11.008.

(59) Van Ryswyk, H.; Ellis, A. B. Optical Coupling of Surface Chemistry. Photoluminescent Properties of a Derivatized Gallium Arsenide Surface Undergoing Redox Chemistry. *J. Am. Chem. Soc.* **1986**, *108* (9), 2454–2455. https://doi.org/10.1021/ja00269a058.